A comparison between the long-time self-diffusion and low shear viscosity of concentrated dispersions of charged colloidal silica spheres

A. Imhof and A. van Blaaderen
Van't Hoff Laboratory, University of Utrecht, Padualaan 8, 3584 CH Utrecht, The Netherlands

G. Maret
Hochfeld Magnetlabor, Max Planck Institut für Festkörperforschung, 166x, F 38042, Grenoble, France

J. Mellema
Rheology Group, Department of Applied Physics, University of Twente, 7500 AE Enschede, The Netherlands

J. K. G. Dhont
Van't Hoff Laboratory, University of Utrecht, Padualaan 8, 3584 CH Utrecht, The Netherlands

(Received 8 September 1993; accepted 14 October 1993)

Measurements are presented of the long-time self-diffusion coefficient and of the low shear limiting viscosity of dispersions of charge stabilized colloidal silica spheres. Long-time self-diffusion coefficients were measured using fluorescence recovery after photobleaching (FRAP), the theory of which is presented and generalized to Gaussian laser beams. The particles, suspended in solutions of LiCl in dimethylformamide, interacted via a screened Coulomb potential, the range of which was varied through the ionic strength. Measurements were made up to volume fractions beyond freezing where a coexistence occurred between a colloidal crystal and a colloidal fluid. It is often speculated that the long-time self-diffusion coefficient and the low shear viscosity of a dispersion are related through a simple Stokes–Einstein-like relation, but this expectation is not confirmed by the experiments. A slightly modified relation, however, does seem to provide a reasonable empirical description of the data.

I. INTRODUCTION

The measurement of particle motions in concentrated colloidal dispersions provides an important test of statistical mechanical and hydrodynamic many-body theories. The most frequently applied technique to study microscopic dynamics is dynamic light scattering (DLS). With this technique, information is obtained primarily about the relaxation of concentration fluctuations, which is a collective process. Only in some cases has it been possible to measure the single particle dynamics using DLS since it places rather stringent demands on the system under study. Kops-Werkhoven *et al.*[1] used the large polydispersity of a refractive index matched hard-sphere system which has the disadvantage of obscuring the interpretation of data. Van Megen *et al.*[2] and Ottewill *et al.*[3] used strongly scattering hard-sphere tracer particles in a concentrated dispersion of index matched hard-sphere host particles. Recently, Härtl *et al.*[4] reported on analogous experiments on a tracer/host system of charged spheres. It is clear, however, that it is often not possible to find a suitable tracer system since the particles should have identical interactions, although their scattering properties must be quite different.

In this paper, we use fluorescence recovery after photobleaching (FRAP) to measure the long-time self-diffusion coefficient (D_s^L). The advantage of using this technique is that it does not place the aforementioned restrictions on the system. Since it does not rely on scattering, the results are much less sensitive to polydispersity in the particle size. Furthermore, with FRAP, one is certain to do measurements in the long-time limit, which can be a matter of some concern in DLS. Measurements of D_s^L with FRAP have been reported for charged spheres as a function of ionic strength at a given volume fraction[5] and for both hard and charged spheres at different ionic strengths as a function of volume fraction.[6]

In this work, we investigate the relation between D_s^L and the low shear limiting viscosity $\eta_{\dot{\gamma}\to 0}$ of dispersions of fluorescently labeled charged silica spheres suspended in solvents differing in ionic strength. It is well known that for a Brownian particle suspended in a liquid, there exists a simple relation between the particle's diffusion coefficient D_0 and the friction factor f, the Einstein relation[7]

$$D_0 = kT/f, \tag{1}$$

where k is Boltzmann's constant and T is the absolute temperature. For a sphere of radius a suspended in a liquid of viscosity η_0, the friction factor is given by Stokes's formula

$$f = 6\pi\eta_0 a. \tag{2}$$

A combination of the two then leads to the Stokes–Einstein relation

$$D_0 = \frac{kT}{6\pi\eta_0 a}. \tag{3}$$

This relation is only valid for dilute dispersions, where interactions between Brownian particles can be neglected. Is there a relation between diffusion and viscosity for interacting systems, similar to Eq. (3)? It was recently found experimentally[6] that for hard spheres, there is a remarkable similarity between D_s^L and the inverse of the low shear

 0021-9606/94/100(3)/2170/12/$6.00

viscosity $\eta_{\dot{\gamma}\to 0}$ of the dispersion over a large range of volume fractions. For micelles, this similarity has also been noted.[8] Physically the following interpretation can be given. If a Brownian particle is moving through a concentrated dispersion for some time, it is feeling on average a net friction force arising not only from the solvent, but from the interactions with other Brownian particles as well. Assuming that the total friction force now obeys the Stokes Eq. (2), with η_0 replaced by the dispersion viscosity $\eta(\phi)$, one obtains

$$D_s^L(\phi)=\frac{kT}{6\pi\eta_{\dot{\gamma}\to 0}(\phi)a}, \tag{4}$$

where the dependence on volume fraction ϕ has been made explicit. The subscript $\dot{\gamma}\to 0$ implies that the viscosity should be taken in the limit of infinitely small shear rates. For atomic and molecular liquids, this relation is widely used and known from experiment to be rather accurate, although the factor of 6 in Eq. (4) should be replaced by a factor of about 3.[9] In electrolyte solutions, the reciprocal relation between self-diffusion and viscosity is known as the Walden rule. Theoretically, there has been some effort to derive such a relation for both atomic fluids[10] and colloidal dispersions.[11]

The aim of this paper is to establish the accuracy of the "generalized Stokes–Einstein relation" (4) for systems with various pair interaction potentials. In Sec. II, we will first give a short account of Brownian motion and relevant particle interactions. We shall also present a theoretical description of the FRAP experiment, which is an extension of the existing theory.[12] We first show that the kind of diffusion measured with FRAP is self-diffusion and we then calculate the FRAP signal for the case of a Gaussian laser beam profile. Section III contains the experimental details and Sec. IV contains the results and discussion. Finally, in Sec. V, the conclusions are summarized.

II. THEORY

A. Self-diffusion

A colloidal particle suspended in a liquid will execute a Brownian motion due to the impacts of many solvent molecules. The phase coordinates of the solvent molecules fluctuate on a much shorter time scale than those of the Brownian particle because of the large mass and size difference. The velocity of a particle of mass m fluctuates with a characteristic fluctuation time

$$\tau_B=\frac{m}{f}, \tag{5}$$

where f is the Stokes friction factor. In this time interval, the particle moves only over a small fraction of its radius. Over times $t\gg\tau_B$, its velocity is completely relaxed so that it moves diffusively. τ_B defines the Brownian or diffusive time scale. The mean-square displacement is now a linear function of time

$$\langle|\mathbf{r}(t)-\mathbf{r}(0)|^2\rangle=6D_0t, \quad t\gg\tau_B, \tag{6}$$

where $\mathbf{r}(t)$ is the position coordinate of the Brownian particle at time t. For interacting particles, things are more complicated. First, particles influence each other by disturbing the solvent flow field through which they move. These hydrodynamic interactions operate on a time scale τ_H which is usually of the same order as τ_B, so that they act instantaneously on the Brownian time scale. Also, the particles can have potential interactions with each other such as (shielded) Coulomb, excluded volume, and van der Waals interactions. To include these in the discussion, a time scale τ_I is usually introduced. The interaction time scale is a typical time needed for a particle to diffuse over such a distance that it feels a substantial change of the potential interaction forces from the other particles; this distance is of the order of the location of the main peak of the pair-correlation function. On times $\tau_B\ll t<\tau_I$, the particle diffuses, on the average, in a potential minimum of the neighboring particles, so that its mean-square displacement is only influenced by hydrodynamic forces. This defines the so-called short-time self-diffusion coefficient D_s^S

$$\langle|\mathbf{r}(t)-\mathbf{r}(0)|^2\rangle=6D_s^St, \quad \tau_B\ll t\ll\tau_I. \tag{7}$$

On this time scale, the particle moves over only a very small fraction of its radius. On time scales greater than τ_I, also the direct interactions between particles play an important role. A particle then needs to distort the configuration of neighboring particles, causing it to slow down. The mean-square displacement then defines the long-time self-diffusion coefficient D_s^L

$$\langle|\mathbf{r}(t)-\mathbf{r}(0)|^2\rangle=6D_s^Lt, \quad t\gg\tau_I. \tag{8}$$

Experiments with DLS[2] seem to indicate that this limit is reached already after, typically, a few tenths of a second, although at higher volume fractions, this means that the particle has moved over only about one particle radius. The long-time self-diffusion coefficient is the quantity that is measured with FRAP, as will be shown later on.

There are relatively little theoretical results for D_s^L as the problem of calculating it is extremely complicated, especially because of the hydrodynamic interactions involved. For hard spheres, Batchelor,[13] and later Cichocki and Felderhof with a more accurate description of hydrodynamic interactions, calculated the first order in volume fraction ϕ coefficient[14]

$$D_s^L=D_0(1-2.10\phi). \tag{9}$$

In addition, there are a few theoretical results for higher volume fractions that neglect hydrodynamic interactions[15] and Brownian dynamics computer simulations,[16] all for hard spheres. Finally, the interesting proposal by Medina-Noyola[17] should be mentioned, which decouples hydrodynamic effects from potential interactions

$$D_s^L=D_s^SD_s^H/D_0, \tag{10}$$

where D_s^H is the long-time self-diffusion coefficient if one neglects hydrodynamic interactions. This method yields erroneous results at low ϕ, but is expected to be rather accurate at higher ϕ.

As mentioned in the Introduction, one possible approach for high volume fractions would be to generalize the Stokes–Einstein relation, as in Eq. (4). However, for low volume fractions of hard spheres, Einstein[7] showed that

$$\eta=\eta_0(1+2.5\phi). \tag{11}$$

Comparison with Eq. (9) shows that Eq. (4) cannot be exact. Moreover, the factor 2.5 in Eq. (11) is independent of the type of interaction between the particles, in contrast to the first order in ϕ term in Eq. (9). Nevertheless, it is hoped that for higher volume fractions, there does exist a Stokes–Einstein-like relation between η and D_s^L.

B. Particle interactions

For charged spheres, the relevant interactions are described by the hard core repulsion and the Derjaguin–Landau–Verwey–Overbeek (DLVO) potential consisting of an electrostatic repulsion and a van der Waals attraction.[18] When the particles are at a center to center distance r, we write

$$V(r)=V_R(r)+V_A(r) \tag{12}$$

with the repulsive part $V(r)$ approximated as

$$V_R(r)=\begin{cases}\infty, & (r<2a)\\ 2\pi\epsilon a\psi_0^2\ln\{1+\exp[-\kappa(r-2a)]\}, & (r\geqslant 2a)\end{cases} \tag{13}$$

and the attractive part as

$$V_A(r)=-\frac{A}{6}\left[\frac{2a^2}{r^2-4a^2}+\frac{2a^2}{r^2}+\ln\left(\frac{r^2-4a^2}{r^2}\right)\right]. \tag{14}$$

Here, ϵ is the solvent permittivity, ψ_0 is the particle surface potential, A is the Hamaker constant, and κ is the inverse Debye screening length. κ is determined by the concentrations c_i and charges z_i of the ionic species in solution as follows:

$$\kappa^2=\frac{e^2N_A}{\epsilon kT}\sum_i c_iz_i^2 \tag{15}$$

with e the elementary charge and N_A Avogadro's number.

The particle charge Q can be written as

$$Q=4\pi\epsilon\frac{kT}{e}\kappa a^2\left[2\sinh(\psi/2)+\frac{4}{\kappa a}\tanh(\psi/4)\right], \tag{16}$$

where $\psi=\psi_0e/kT$.

The Debye screening length and the particle hard-core diameter set the range and softness of the pair-interaction potential. In our experiments, we will vary κ by adding salt [see Eq. (15)]. Relation (16) will be used to determine the charge on the particles from electrophoretic mobility measurements.

C. Fluorescence recovery after photobleaching

In FRAP, first a well-defined part of the sample is illuminated by an intense laser light pulse. This irreversibly destroys the fluorescence of a certain fraction of the fluorophore molecules, which are chemically attached to the surface or inside the core of the Brownian particles. This process is called photobleaching. After the short pulse, the intensity of the incident radiation is greatly reduced, so that subsequent bleaching is insignificant. The fluorescent intensity is now monitored as a function of time. The bleach pattern gradually fades away as a result of diffusion of the labeled species, giving rise to a change in the measured fluorescent intensity. The rate at which this process takes place is related to the species' diffusion coefficient.

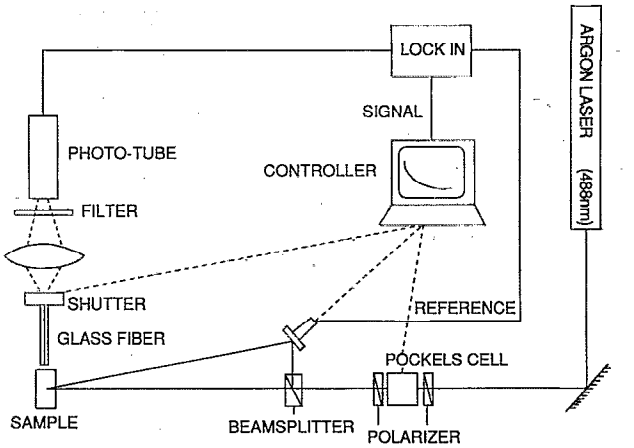

FIG. 1. A schematic picture of the FRAP setup.

The FRAP technique was originally used with a spot as the bleach pattern,[19] but later improvements used a sinusoidal fringe pattern created by either a diffraction grating[20] or by interference of two laser beams.[12] The apparatus used here is essentially the one developed by Davoust *et al.*[12] and is depicted schematically in Fig. 1. The bleached pattern is realized by splitting a laser beam and recombining the two resulting beams under some small angle 2θ using a beam splitter and a mirror. The resulting sinusoidal intensity profile is shown at the top of Fig. 2. Photobleaching leaves an (approximately) sinusoidal dye concentration distribution (the middle of Fig. 2). It is a consequence of the diffusion equation that the bleach pattern remains sinusoidal with an amplitude decreasing exponentially in time. After bleaching, the pattern is monitored by the same fringe pattern with a reduced intensity (the lower part of Fig. 2). This reduction is brought about by suddenly changing the voltage over the Pockels cell. This causes the plane of polarization of the exiting beam to rotate to a new orientation for which the analyzer is less transparent. In Fig. 2, the crests in the monitoring intensity coincide with troughs in unbleached dye concentration. Since these regions give the most fluorescence, the total fluorescent intensity is seen to rise exponentially. During the monitoring phase the fluorescent intensity is recorded by a photomultiplier tube via a glass fiber and a filter that admits only the fluorescent wavelengths.

A further improvement on the original FRAP technique consists of giving one of the two incident beams a phase difference by reflecting it off a piezoelectrically driven mirror which oscillates in a direction normal to its surface.[12] This causes the monitoring fringe pattern to move periodically over the bleach pattern with a well-

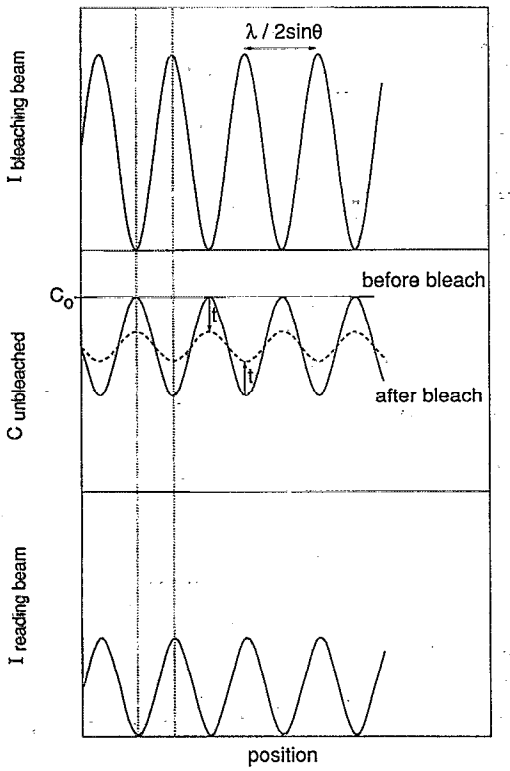

FIG. 2. A sketch of the bleaching (top) and reading (bottom) intensity profiles and the unbleached dye concentration (middle).

known frequency (typically 1 kHz). The measured fluorescent intensity is now modulated with this frequency as the bleach pattern and the monitoring fringes fall into and out of phase. The envelope of the intensity is extracted from the total fluorescence by a lock-in amplifier. This process reduces the noise caused by the often large background fluorescence.

In the following, a detailed theoretical analysis of FRAP is given taking into account the Gaussian beam profile that is present for most lasers working in the TEM_{00} mode. A simpler analysis assuming infinitely wide beams has been given in Ref. 12. We shall also show rigorously that with FRAP, true self-diffusion is measured. This is a direct consequence of the fact that after bleaching, the particles remain identical with respect to their interactions.

In the following description, we take the origin at the point of intersection of the crossed beams, with the z direction along the bisector and the x direction in the plane defined by the beams. It can then be easily shown that the intensity field of the interference pattern is given by

$$I(\mathbf{r},t')=I^0\exp[-2w^{-2}(x^2\cos^2\theta+y^2)]\times\{1+\cos[k_0x+\phi(t')]\},\quad(17)$$

where w is the e^{-2} radius of the Gaussian beams. Furthermore,

$$k_0=\frac{4\pi}{\lambda}\sin\theta\quad(18)$$

and $\phi(t')$ describes the time-dependent phase difference between the two beams, which is usually sinusoidal. For not too large θ, the z dependence of $I(\mathbf{r},t')$ is negligible. The fringe spacing L equals $2\pi/k_0$ and is thus given by

$$L=\frac{\lambda}{2\sin\theta}.\quad(19)$$

It is also useful to define the number of fringes N as the quotient of the e^{-2} width (in the x direction) of the region where the two beams overlap and the fringe spacing, so that from Eqs. (17), (18), and (19)

$$N=2\left(\frac{w}{\cos\theta}\right)\Big/\left(\frac{\lambda}{2\sin\theta}\right)=\frac{4w}{\lambda}\tan\theta=\frac{k_0w}{\pi\cos\theta}.\quad(20)$$

Now consider a system of N_p identical Brownian particles in a volume V, each initially containing n_0 unbleached molecules of a fluorescent dye. The bleach pulse has position-dependent intensity $I_b(\mathbf{r})$ given by Eq. (17) with $\phi(t')\equiv0$ and a duration Δt, which is so short that the particles do not move significantly from their initial positions $\mathbf{r}_i(0)$ during bleaching. We assume irreversible first order kinetics for the photobleaching process, so that the number of unbleached molecules M around position $\mathbf{r}$ satisfies

$$\frac{d}{dt}M(t)=-\alpha M(t)I_b(\mathbf{r}),\quad 0\leqslant t\leqslant\Delta t,\quad(21)$$

where α is the photolytic rate constant. It follows that after the bleach pulse, the number of unbleached molecules in particle i at position $\mathbf{r}_i(0)$ equals

$$n[\mathbf{r}_i(0)]=n_0\exp\{-\alpha\Delta tI_b[\mathbf{r}_i(0)]\},\quad i=1,\ldots,N_p$$
$$=n_0\exp(-K\exp\{-2w^{-2}[x_i^2(0)\cos^2\theta+y_i^2(0)]\}\times\{1+\cos[k_0x_i(0)]\}).\quad(22)$$

The constant $K=\alpha\Delta tI_b^0$ which measures the extent of bleaching, is sometimes called the mean bleaching efficiency index. Note that n is a function of position, which is to be evaluated at the initial position of a particle i. This function is called the bleach pattern and is in fact the initial condition for the diffusion process.

After the bleach pulse, the sample is illuminated by the (time and position dependent) monitoring intensity $I_m(\mathbf{r},t')$, again given by Eq. (17). The fluorescent intensity emitted by a particle at position $\mathbf{r}_i(t)$ is proportional to the number of fluorescent molecules $n[\mathbf{r}_i(0)]$ contained in it and to the local intensity $I_m[\mathbf{r}_i(t),t']$. Summing the contributions of all particles, one obtains for the instantaneous fluorescent intensity emitted by the sample

$$I_f(t,t')=Q\sum_{i=1}^{N_p}n[\mathbf{r}_i(0)]I_m[\mathbf{r}_i(t),t'],\quad t>\Delta t,\quad(23)$$

where Q is the product of the quantum efficiencies for light absorption and emission. It has been tacitly assumed that the variation of the intensity over one particle is negligible, which is always the case in FRAP. Note that the expression in Eq. (23) does not contain any interference terms because the fluorescent light is incoherent.

We may reasonably assume that bleaching of fluorophore molecules does not influence the pair-interaction potential of the particles, so that all the particles remain statistically identical after bleaching. For large N_p in Eq. (23), we may then write I_f as an ensemble average over the initial positions and the positions at time t of all particles

$$I_f(t,t')=QN_p\int_V d\mathbf{r}'\int_V d\mathbf{r}\, n(\mathbf{r}')I_m(\mathbf{r},t') \times P(\mathbf{r}'|t=0)P(\mathbf{r}',\mathbf{r}|t). \quad (24)$$

Here, we have written $\mathbf{r}'=\mathbf{r}_i(0)$ and $\mathbf{r}=\mathbf{r}_i(t)$. Furthermore, $P(\mathbf{r}'|t=0)$ is the probability density of finding a given particle at position $\mathbf{r}'$ at time $t=0$ and $P(\mathbf{r}',\mathbf{r}|t)$ is the conditional probability density that, given a certain particle at $\mathbf{r}'$ at time zero, it is found at $\mathbf{r}$ at time t. The occurrence of the latter function implies that the type of diffusion measured with FRAP is indeed self-diffusion. If the system was in equilibrium before bleaching, then $P(\mathbf{r}'|t=0)=1/V$, where V is the volume of the system. $I_m(\mathbf{r},t')$ and $n(\mathbf{r})$ are both independent of the z coordinate over a distance d, the thickness of the sample cell, so that the z integration in Eq. (24) can be performed right away yielding a factor of d. We are then left with a two-dimensional integral over $\mathbf{R}=(x,y)$. Since the system remains statistically invariant under translations in the x and y directions, we have $P(\mathbf{R}',\mathbf{R}|t)=P(\mathbf{R}-\mathbf{R}'|t)$. We then get

$$I_f(t,t')=Q\rho d\int_{R^2} d\mathbf{R}'\int_{R^2} d\mathbf{R}\, n(\mathbf{R}')I_m(\mathbf{R},t') \times P(\mathbf{R}-\mathbf{R}'|t), \quad (25)$$

where $\rho=N_p/V$ is the particle number density. Upon applying the convolution theorem for Fourier transforms to the pair of functions $n(\mathbf{R}')$ and $P(\mathbf{R}-\mathbf{R}'|t)$, we obtain

$$I_f(t,t')=2\pi Q\rho d\int d\mathbf{q}\, n(\mathbf{q})I_m(-\mathbf{q},t')P(\mathbf{q}|t). \quad (26)$$

Here, the Fourier transform of a function $f(\mathbf{r})$ is defined by

$$f(\mathbf{q})=(2\pi)^{-n/2}\int d\mathbf{r}\, f(\mathbf{r})e^{i\mathbf{q}\cdot\mathbf{r}}, \quad (27)$$

where n is the dimension, in this case 2. Equation (26) is the general expression for the fluorescence recovery signal in terms of the Fourier transforms of the bleach pattern $n(\mathbf{R})$, the monitoring intensity $I_m(\mathbf{R},t')$, and the probability density $P(\mathbf{R}|t)$ for the displacement $\mathbf{R}$ of a Brownian particle in time t.

The transport process that we want to study with FRAP is described by a Smoluchowski type equation for the function $P(\mathbf{R}|t)$. Since the fringe spacing L given by Eq. (19) is always much larger than the particle diameter, the relevant process is long-time self-diffusion described by

$$\frac{\partial P(\mathbf{R}|t)}{\partial t}=D\left(\frac{\partial^2}{\partial x^2}+\frac{\partial^2}{\partial y^2}\right)P(\mathbf{R}|t), \quad P(\mathbf{R}|t=0)=\delta(\mathbf{R}), \quad (28)$$

where D is the long-time self-diffusion coefficient and δ is the Dirac delta distribution. This problem may be easily solved by Fourier transformation into $\mathbf{q}$ space with the result

$$P(\mathbf{q}|t)=(2\pi)^{-1}e^{-Dq^2t}. \quad (29)$$

Equation (26) may now be integrated explicitly yielding

$$I_f(t,t')=A\left\{I_0^*(K,N,Dt)+I_1^*(K,N,Dt)\cos\phi(t') \times\exp\left[-Dk_0^2t\Big/\left(1+\frac{8Dt\cos^2\theta}{w^2}\right)\right]\right\} \quad (30)$$

with

$$A=QI^0n_0\rho\frac{\pi dw^2}{2\cos\theta},$$

$$I_0^*(K,N,Dt)=\frac{2}{\pi}\int d\xi\int d\eta\exp[-Kf(a\xi,b\eta,N)] \times\exp[-2(\eta^2+\xi^2)],$$

$$I_1^*(K,N,Dt)=\frac{2}{\pi}\int d\xi\int d\eta\exp[-Kf(a\xi,b\eta,N)] \times\exp[-2(\eta^2+\xi^2)]\cos(\pi N\xi),$$

$$f(\xi,\eta,N)=\exp[-2(\xi^2+\eta^2)][1+\cos(\pi N\xi)],$$

$$a=(1+8Dt\cos^2\theta/w^2)^{1/2}, \quad b=(1+8Dt/w^2)^{1/2}.$$

From Eq. (30), we see that the total fluorescent intensity consists of two parts. The first is a constant "background" fluorescence. The second part is modulated by the cosine of the phase angle $\phi(t')$ and can thereby be picked up by the lock-in amplifier. It falls off almost exponentially when $w/\cos\theta$ is large compared to Dt. Since $w/\cos\theta$ is the width of the region of overlapping beams and $6Dt$ is the mean square displacement, the ratio of the two measures the diffusion of particles into and out of the overlap region, which competes with the diffusion of particles diffusing into and out of fringes. We shall now derive a condition under which the former process is negligible. Note that we can generally write $\exp[-x^2/(1+\delta)]=\exp(-x^2)\times\exp[x^2\delta/(1+\delta)]$. This is approximately equal to $\times\exp(-x^2)$ if $x^2\delta/(1+\delta)<0.01$ or equivalently $1/\delta>100x^2-1$. When this is applied to the exponential in Eq. (30), it becomes a simple $\exp(-Dk_0^2t)$ under the constraint that

$$w^2/8Dt\cos^2\theta>100Dk_0^2t-1. \quad (31)$$

This can be solved for Dk_0^2t yielding

$$Dk_0^2t<\frac{2^{1/2}}{40}\frac{k_0w}{\cos\theta}=\frac{2^{1/2}\pi}{40}N. \quad (32)$$

For good data fitting, one needs to measure the exponent up to, say, $Dk_0^2t=3$, which implies that the number of fringes should be about 30 or more. It is seen that under the same constraint, all the exponentials in I_0^* and I_1^* can be simplified yielding the final result

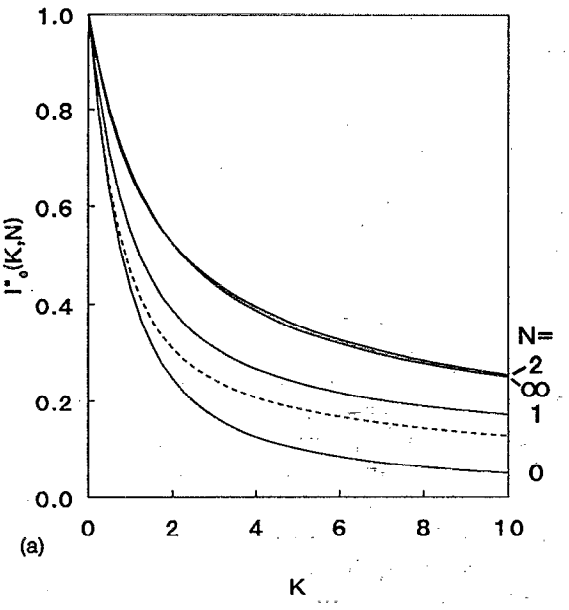

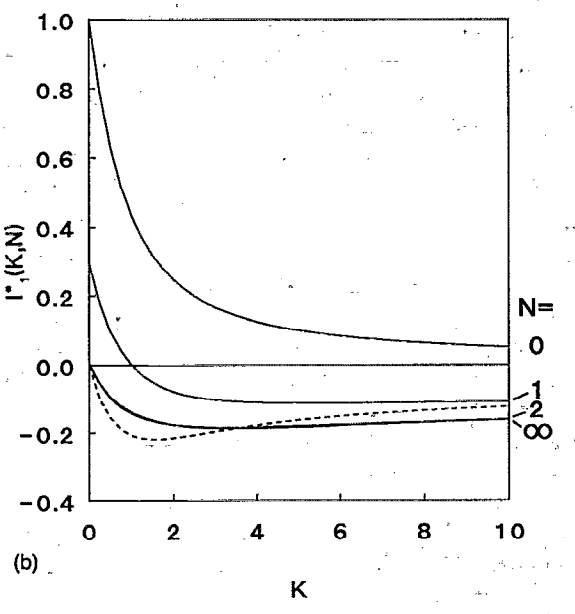

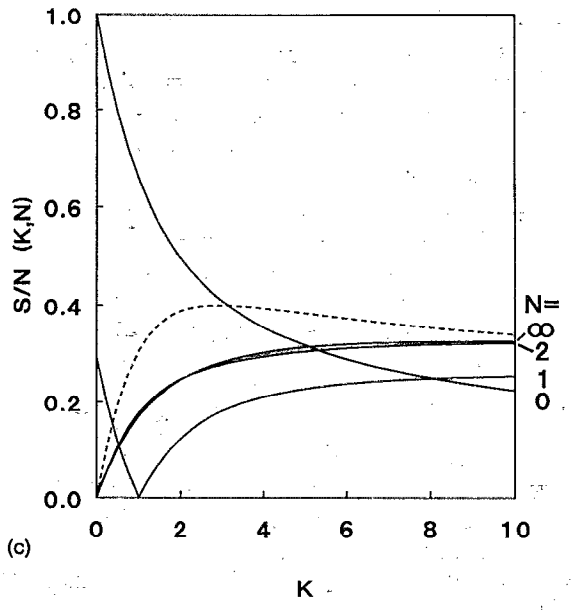

FIG. 3. The functions (a) $I_0^*(K,N)$; (b) $I_1^*(K,N)$; and (c) S/N for several values of N (solid lines) and from Ref. 12 (dashed line).

$$I_f(t,t') = QI^0 n_0 \rho \frac{\pi dw^2}{2\cos\theta}\,[I_0^*(K,N) + I_1^*(K,N)\cos\phi(t')e^{-Dk_0^2 t}] \tag{33}$$

with

$$I_0^*(K,N) = \frac{2}{\pi}\int d\xi \int d\eta \exp[-Kf(\xi,\eta,N)] \times \exp[-2(\xi^2+\eta^2)], \tag{34a}$$

$$I_1^*(K,N) = \frac{2}{\pi}\int d\xi \int d\eta \exp[-Kf(\xi,\eta,N)] \times \exp[-2(\xi^2+\eta^2)]\cos(\pi N\xi). \tag{34b}$$

Note that $n_0\rho dw^2/\cos\theta$ is approximately the (average) number of fluorescent molecules in the volume that is illuminated by both beams at the same time. The integrals $I_0^*(K,N)$ and $I_1^*(K,N)$ determine the ratio of decaying to total fluorescence and can be calculated either numerically or analytically after Taylor expansion of the first exponent in the integrands.

We see from Eq. (33) that only a part of the fluorescence, given by I_1^*, is measured after lock-in detection, but the unmodulated fluorescence I_0^* gives rise to noise caused by the Poisson statistics over the total number of photons collected by the detector. This noise is uniform over all frequencies and proportional to the square root of the number of photons. It is therefore useful to study the signal-to-noise ratio S/N

$$\mathrm{S/N} \sim \frac{|I_1^*(K,N)|}{[I_0^*(K,N)]^{1/2}}. \tag{35}$$

In Fig. 3, I_0^*, I_1^*, and S/N are plotted as functions of K for various values of N and compared with the results that were obtained by Davoust *et al.*[12] for infinitely wide laser beams. It is seen that for these functions, the limit of a

large number of fringes is reached already for $N>2$. In this limit, the results obtained here do not reduce to the results of Davoust *et al.*[12] Also, these authors find that it would be best to use $K\approx 2$, where the signal-to-noise ratio is maximal. For Gaussian beams, the curve becomes relatively flat for $K>3$ and the maximum is shifted to $K\approx 9.5$, but is much less pronounced. The discrepancy between our results and those of Ref. 12 is probably the result of an unallowed interchange of the integration and the limit $w\to\infty$. In the above discussion, w is kept finite, while in Ref. 12, w is set equal to infinity from the start, introducing an error in their results.

We want to stress here that the aforementioned assumptions and restrictions—no z dependence of the intensity, no light scattering, no movement of the particles during the bleach pulse, and first order kinetics of the bleaching process—were made only to make quantitative calculation possible. These assumptions are not necessary for a good FRAP measurement, because it follows from Eq. (26) that if the fringe pattern is sinusoidal, then only one Fourier component of the concentration profile is picked out, of which the (exponential) decay is monitored. The processes mentioned only affect the exact form of S/N.

In summary, the conclusions are that (i) FRAP measures self-diffusion under the constraint that particle interactions are not affected by bleaching; (ii) at least 30 fringes are needed to obtain a single exponential decay; and (iii) for an optimal signal-to-noise ratio, the mean bleaching efficiency index K should be greater than, say, 2.

III. EXPERIMENT

A. Particle preparation and characterization

Colloidal silica particles were synthesized following the procedure of Stöber *et al.*[21] Using the usual seeded growth technique, the particles were first grown to a radius of 208 nm as determined by static light scattering. The resulting system consisted of 70 g of silica suspended in a mixture of 160 ml, 25% ammonia and 1840 ml of ethanol. These particles were fluorescently labeled using the method of Van Blaaderen *et al.*[22] To this end, 0.0849 g of fluorescein isothiocyanate (FITC, Sigma) was dissolved in 0.938 g distilled 3-(aminopropyl)triethoxysilane (APS, Janssen) and the mixture was stirred for 24 h in a dried flask. Subsequently, the reaction product was dissolved in 9.0 ml of absolute ethanol. Then 3.5 ml of this solution and 10 ml of tetraethoxysilane (TES, Fluka) were added to the silica sol, which was then stirred for 24 h. In our case, this corresponded to about 50×10^3 FITC molecules per particle. The extra addition of TES facilitated incorporation of the fluorophore in the particles and made the particles grow to 211 nm as measured by static light scattering. The resulting particles therefore carry a thin outer shell of about 3 nm of silica containing all the fluorophore.

Excess reactants were removed by slow centrifugation and redispersion in ethanol. The dispersion was divided in three batches and the solvent was changed to dimethylformamide (DMF, Baker) with different ionic strengths by repeated centrifugation and redispersion in the desired solvent. In this way, dispersions were obtained in pure DMF, in 1.006×10^{-3} M LiCl in DMF, and in 0.1005 M LiCl in DMF, respectively. Even for the highest salt concentration, the dispersions remained stable for over a year.

TABLE I. Particle characterization results.

Radius (nm)	(SLS)	211±1	
	(DLS)	213±3	
	(TEM)	187	Polydispersity 0.040
Refractive index		1.451	(ethanol/2-bromoethanol)
(λ=546 nm)		1.449	(DMF/2-bromoethanol)
Density (g/cm^3)		2.02±0.03	

For each of the three systems, concentrated stock dispersions were obtained by letting the particles sediment and then decanting an amount of solvent. The volume fractions of these dispersions were determined by measuring the dispersion density in a measuring flask and the silica weight fraction by drying a weighted amount of dispersion at 80 °C under nitrogen and reweighing. For all measurements, samples of lower volume fraction were prepared by dilution of a weighted amount of stock dispersion with a weighted amount of solvent. In this way, the ionic strength of the solvent was kept constant throughout the volume fraction range (neglecting counterion dissociation). This is in contrast to the experiments in Ref. 6, where the salt concentration in the solvent increases with the volume fraction.

The results of the particle characterization are presented in Table I. Static light scattering (SLS) was performed on a Fica 50 photometer on very dilute suspensions in ethanol at a wavelength of 546 nm. A 546 nm bandpass filter was used to eliminate the (small) fluorescent contribution to the scattered radiation. The measured scattering curve was fitted to theoretical curves calculated using the Mie scattering coefficients. Dynamic light scattering (DLS) was done on dilute samples in DMF at 25.0 °C at a wavelength of 647.1 nm using a Krypton laser (Spectra Physics model 2020). Electron micrographs were made on a Philips EM301 electron microscope and analyzed with interactive image analysis (IBAS). About 350 particles were measured to obtain a mean radius and a polydispersity (defined by the standard deviation divided by the mean). For the silica system, one systematically finds a smaller particle radius which is attributed to shrinkage under the severe circumstances in the transmission electron microscopy (TEM) chamber. The refractive index of the particles was measured at 20 °C with an Abbe refractometer at the point of maximum transmission of 546 nm radiation of a sample dispersed in a suitably chosen solvent mixture (see Table I). The particle mass density was determined several times by drying a known weight of a concentrated dispersion of known density.

Some relevant properties of the three dispersions in DMF with different salt concentration are given in Table II. Solvent viscosities were measured with an Ubbelohde capillary viscometer. Diffusion coefficients at infinite dilution were measured with DLS on very dilute suspensions. The variation in D_0 can be explained completely by the variation in solvent viscosity, so there is no contribution of

TABLE II. Some dispersion properties.

[LiCl] (M)	η_0 (mPa)	D_0 (10^{-12} m^2/s)	κa	Conductivity (S/m)	Mobility (10^{-8} m^2/V s)	ψ_0 (mV)	Q (mC/m^2)
1.35×10^{-5}	0.798	1.27±0.03	2.64	1.08×10^{-4}	−2.35	< −130	< −1.4
1.006×10^{-3}	0.799	1.28±0.04	31.6	6.26×10^{-3}	−2.77	−83	−6.1
1.005×10^{-1}	0.867	1.20±0.03	230	2.9×10^{-1}			

electrolyte friction for the present values of κa. The values of κa were calculated using Eq. (15). For the salt free system, κa was calculated using an effective 1–1 electrolyte concentration obtained from the solvent conductivity. For the 0.001 and 0.1 M systems, the noncomplete dissociation of LiCl in DMF has to be taken into account. For the 0.001 M solution, the dissociation constant is 0.972.[23] For the 0.1 M system, we do not know the exact value, but it can be estimated at about 0.5 from conductivity. The exact value of κa is inconsequential in this system since κ^{-1} is already smaller than 1 nm. Conductivities and mobilities were measured on dilute suspensions (volume fraction ~0.001) using a Pen Kem system 3000. From these, the surface potential ψ_0 could be calculated[24] and with Eq. (16) the particle charge Q. For the salt free system, only a minimum value for ψ_0 can be given, since for $\kappa a \sim 3$, the mobility becomes an almost constant function of zeta potential.[24] For the 0.1 M system, the mobility could not be measured as for an unknown reason the particles moved diagonally through the sample cell. In a Burton U tube, their mobility was too small to be measured. We prepared a sample in 0.01 M LiCl which also showed this effect, although to a much lesser extent. In samples with a lower salt concentration, this deviation did not occur.

B. Phase diagrams

At higher volume fractions, all three dispersions show a spontaneous phase separation into an ordered crystalline phase (evidenced by bright speckles caused by Bragg reflections) and a disordered fluid-like phase. Depending on the volume fraction, the appearance of the speckles could be observed within a few seconds to a few minutes after vigorously shaking the suspension. The crystallites then start to sediment rather quickly, which completes the phase separation. This makes it possible to determine the relative sizes of the ordered and disordered phases following a procedure devised by Paulin *et al.*,[25] which runs as follows: The particles in the fluid phase sediment along with the crystallites, although much more slowly. As has often been observed, these particles sediment into an ordered lattice, giving rise to growth of the crystalline phase. If one monitors its growth over a period of many days, one observes a linear increase following a nonlinear change due to incomplete sedimentation and inefficient stacking of the crystallites. On extrapolating the linear part to zero time, the effect of sedimentation is ruled out and the true equilibrium crystal fraction is obtained. We carried out these experiments in a thermostatted room using long thin glass vials (Vitro Dynamics, Inc., Rockaway, NJ) of size 100 $\times 4 \times 0.4$ mm^3, in which the height of the sediment could be easily measured. We did not observe a disordered solid phase (a colloidal glass) in any of these experiments, since volume fractions were not high enough.

C. Rheology

The Contraves Low Shear 30 constant shear rheometer was used to measure dispersion viscosities. The apparatus was equipped with a concentric cylinder geometry of outer radius of 12 mm and gap width of 0.5 mm. In this configuration, shear rates in the range 0.01–100 s^{-1} were attainable. The temperature was kept constant at 25.0 °C to within 0.1 °C using a thermostatted bath that circulated water around the couette geometry. The apparatus was calibrated in the relevant viscosity range using Newtonian calibration oils (NMI Delft, The Netherlands) of known viscosity.

For each of the three systems, the flow curve (viscosity vs shear rate) was measured over a range of volume fractions. After homogenization of the sample, a measurement was started at the lowest shear rate, where a torque was still measurable and continued up to shear rates where considerable shear thinning occurred. In this way, it was made certain that the low shear Newtonian plateau was reached; the low shear limiting viscosity $\eta_{\dot{\gamma}\to 0}$ is given by level of that plateau. An example is shown in Fig. 4 for the 0.001 M LiCl system at various volume fractions. This graph displays the effect of shear thinning, caused by distortion of the equilibrium microstructure, occurring at

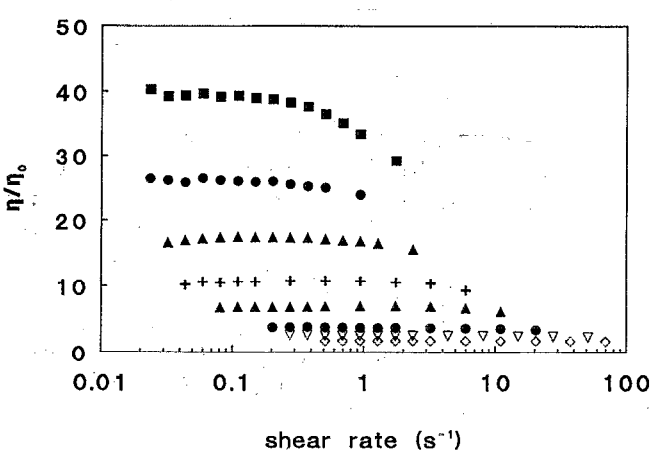

FIG. 4. Some flow curves for the 0.001 M LiCl system. Volume fractions are (from upper to lower lines) 0.3103, 0.2931, 0.2795, 0.2601, 0.2188, 0.1797, 0.1303, and 0.0878.

lower and lower shear rates as the volume fraction increases. The viscosities were eventually normalized by the solvent viscosities given in Table II.

For the highest volume fractions, the viscosities diverged at the lowest shear rates. In such cases, it took a long time for the readout to reach a stationary value. These effects were probably caused by nucleation/crystallization during the measurement.

D. Fluorescence recovery after photobleaching

A description of the FRAP setup we used was given in Sec. II C. The bleaching and exciting radiation of wavelength 488 nm was provided by an argon ion laser. For bleaching, we used light pulses of 1–3 s duration at a typical power of 200 mW. We found no influence of the bleach time on the measured diffusion coefficients. During the monitoring phase, the power was reduced by a factor of about 3000. The beam diameter was 1.5 mm. The fringe spacings we used were 23.8 μm for the more dilute samples and 12.1 and 10.0 μm for the concentrated ones.

After careful homogenization, small samples were transferred to long, thin glass cuvettes (Vitro Dynamics, Inc., Rockaway, NJ) of thicknesses of 200 and 400 μm and width of 2 mm. For every sample, at least ten decay curves were measured, which were then fitted to an exponent according to Eq. (33). Using Eq. (18), the value of D_s^L was calculated. All D_s^L values have been normalized by the respective D_0 as measured with DLS (see Table II). Since the samples could not be thermostatted, D_0 values were corrected for temperature differences from 25.0 °C using the Stokes–Einstein relation with a temperature dependent viscosity. Ambient temperatures during FRAP measurements were 22–25 °C in which range we found, using the Ubbelohde viscometer, $d\eta_0/dT=0.010$ mPa/K.

For the highest volume fractions, a spontaneous nucleation of a crystalline phase occurred in the cuvettes. In such cases, care had to be taken to let all crystallites sediment to make possible a measurement of D_s^L in the coexisting fluid phase. In the coexisting solid, D_s^L values were too small to be measured at the fringe spacings we used due to limitations in the apparatus' mechanical stability. A maximum value could be set, however, $D_s^L/D_0<0.004$.

IV. RESULTS AND DISCUSSION

As a demonstration of the bleaching process, we bleached a spot (no fringes) of diameter 1.5 mm in a sample of volume fraction 0.038 (no added salt) for a few seconds and then measured the emitted fluorescent intensity while exciting with the monitoring intensity. This is a measure of the total fluorescence emitted by the bleached spot and remains constant for a long time since diffusion over distances of the order of the beam diameter (1.5 mm) is extremely slow. Then the same spot was bleached again and the process was repeated a number of times. The resulting bleach curve is shown in Fig. 5 and suggests that bleaching happens in roughly two regimes. Relevant for FRAP are only the first few seconds during which time the number of unbleached molecules falls exponentially although, unfortunately, the percentage bleaching remains relatively small. For bleach times longer than a minute, this number decreases only very gradually. So it seems that the FITC molecules can occupy different sites in the silica matrix where they are quite differently stabilized against photobleaching.

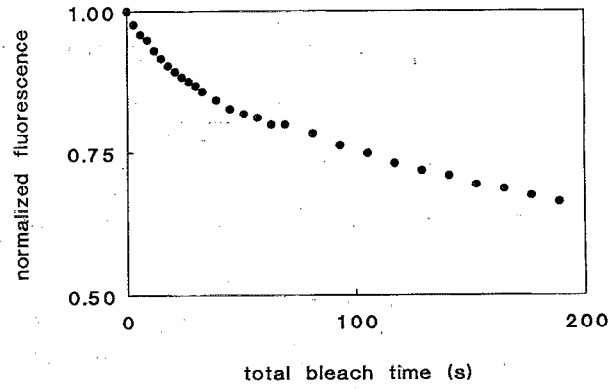

FIG. 5. Bleach curve (fluorescent intensity vs bleach time at 200 mW excitation) for the 0 M LiCl sample at volume fraction 0.038.

In Fig. 6, the results are shown of the measurement of the long-time self-diffusion coefficient and the low-shear limiting viscosity for the three ionic strengths. Figure 6(b) shows the same data as Fig. 6(a), but reciprocally to emphasize the behavior at high volume fractions. For clarity, error bars have not been included in these graphs. However, for the D_s^L values, the error was always found to be $\sim 5\%$. The errors in the viscosities are also estimated at about 5%. For comparison, the hard-sphere data from Ref. 6 are shown in Fig. 6(c).

All curves are seen to extrapolate to unity at low volume fractions. As the D_s^L's have been normalized by D_0 as found with dynamic light scattering, this constitutes an important check on the reliability of the data since in FRAP every disturbance, mechanical or other, will cause the bleach pattern to fade away too quickly, so that the D_s^L values come out too high. We encountered this problem earlier using a much more heavily labeled system with $\sim 10^6$ FITC molecules per particle. At the same experimental conditions, we observed D_s^L rising to 30% in excess of D_0 at the lower volume fractions. Strong absorption of light during the bleach pulse probably gave rise to convections due to local heating. This could not be remedied by using a lower light intensity as the signal then became too small. The particles used in this work were labeled with much fewer FITC molecules and did not give rise to such effects.

The phase diagrams at the top of Fig. 6(b) show the fraction of the system occupied by the crystalline phase as a function of the overall volume fraction of particles. From the linear portion in the coexistence region, the values of the melting and freezing volume fractions can be found by extrapolation. They are given in Table III together with the well-known hard-sphere data from simulation.[26] At the freezing volume fraction ϕ_f, a crystalline phase just begins to form in the fluid phase, whereas at the melting volume

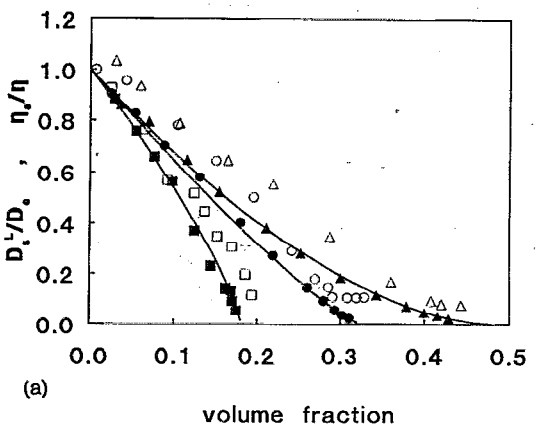

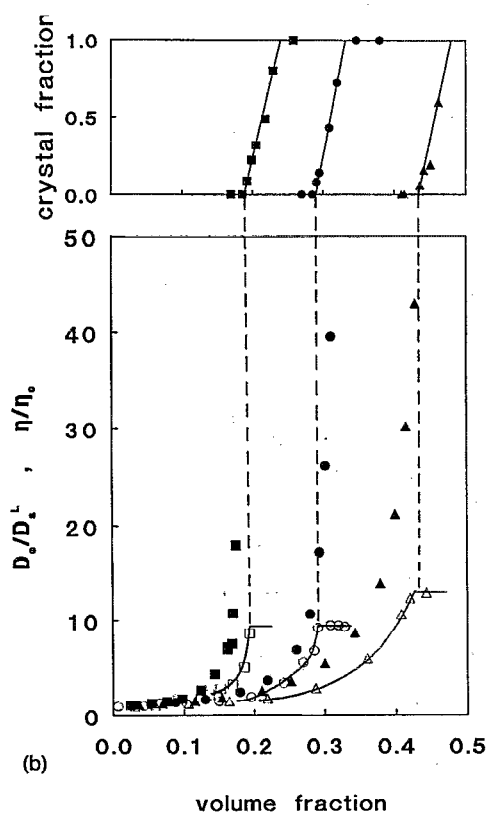

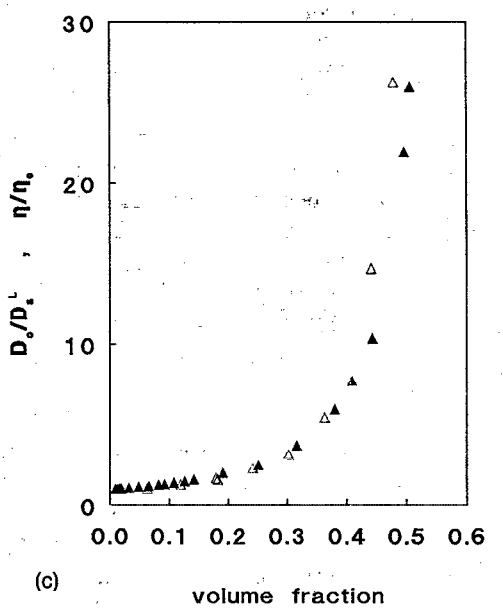

FIG. 6. (a) Diffusion and viscosity data plotted against volume fraction. Open symbols are D_s^L/D_0, filled symbols η_0/η; □—pure DMF; ○—0.001 M LiCl, and △—0.1 M LiCl in DMF. (b) The same as (a), but reciprocal with phase diagrams at the top. Lines are drawn to guide the eye. (c) The same as (b), but with hard-sphere data from Ref. 6.

fraction ϕ_m, all particles have entered the crystalline phase. Figure 6(b) shows that the long-time self-diffusion coefficient rises smoothly with volume fraction and then suddenly levels off to a constant, minimal value at ϕ_f (as measured in the fluid phase). This is understandable, since on crossing the coexistence region, one just increases the amount of crystalline phase, whereas the volume fraction of particles in the fluid phase remains at the constant value of ϕ_f. In the crystalline phase, where diffusion is expected to take place only along grain boundaries and through defect diffusion, the diffusion coefficients were unmeasurably small ($D_s^L/D_0 < 0.004$). It is remarkable that D_s^L in the coexisting fluid is only about ten times smaller than D_0. Evidently the particles are still relatively free to move at ϕ_f. Earlier measurements of D_s^L in a coexisting fluid phase[6] showed a much slower diffusion than our measurements, probably because not enough care was taken to let all crystallites sediment out of the fluid phase.

TABLE III. Freezing (ϕ_f) and melting (ϕ_m) volume fractions of the colloidal systems and for hard spheres (HS) (Ref. 26).

System	ϕ_f	ϕ_m	$\phi_m-\phi_f$
0 M	0.188	0.240	0.052
0.001 M	0.290	0.332	0.042
0.1 M	0.434	0.480	0.046
HS	0.494	0.545	0.051

It is remarkable that the width of the coexistence region $\phi_m-\phi_f$ is independent of the range of the pair potential for our systems (see Table III), whereas it is usually expected to vary in proportion to ϕ_f. Probably, $\phi_m-\phi_f$ begins to decrease only for much smaller values of κa than those for the systems used in the present study. This is also

what the phase diagram of a charged aqueous latex observed by Hachisu *et al.*[27] seems to indicate. It is also remarkable that the 0.1 M system with a double layer thickness below 1 nm does not crystallize at the hard sphere reference value (Table III). However, recently it has been convincingly shown by measurements with the surface force apparatus that silica in water has a tightly bound surface layer of water molecules with a thickness of about 4 nm.[28] DMF resembles water in many of its structural properties.[29] It is therefore not unlikely that such a layer is also present in this solvent. This stabilizing layer explains why the particles do not flocculate at this high ionic strength and could increase the effective radius of the particles.

From Fig. 6, it is seen that there exists a finite zero shear rate viscosity even for volume fractions beyond the freezing volume fraction, at least for the 0.001 and 0.1 M systems. The same behavior is also shown by hard spheres.[30] Physically this means that dispersions that at equilibrium show a disorder–order transition can still support a steady (though small) rate of deformation.

It is seen from Fig. 6 that D_s^L/D_0 and η_0/η qualitatively follow the same trend, but that the latter has a stronger dependence on volume fraction. Also in Fig. 6(a) the D_s^L/D_0 curves seem to be slightly more convex than the η_0/η curves. The generalized Stokes–Einstein relation therefore does not hold. However, the relative deviation is no more than a factor of the order of 2. The curves can be more closely compared if we rescale the volume fractions of the D_s^L curves so that they give a good superposition with η at the divergent part (see Fig. 7). This figure shows that for the 0 M sample, there is a good superposition over the entire ϕ range. For the higher salt concentrations, however, there remains a systematic deviation between the curves of up to 25% for all but the highest volume fractions. The scaling factors used for the 0, 0.001, and 0.1 M systems were 0.850 ± 0.030, 0.920 ± 0.020, and 0.878 ± 0.020, respectively. For the hard sphere data from Ref. 6 (rescaling not shown), the factor would be 1.062 ± 0.020. This does not clearly point to any systematic dependence on the range of interaction.

We tried to explain the data by imagining the friction that is experienced by a particle to consist of two parts. One is the normal Stokes friction due to the solvent molecules. The second contribution is due to neighboring particles that cause a viscosity increase of $\eta-\eta_0$. For the latter part, there is no reason to expect a no-slip boundary condition since the particle is not surrounded by a stationary shell of neighboring particles. Therefore, we write formally

$$f=6\pi\eta_0 a+\nu\pi(\eta-\eta_0)a. \tag{36}$$

Within this iterative picture, we expect ν to have a value in between 4 and b, since for a slip boundary condition, we should expect f to contain a factor of 4π which for no slip would be 6π. Using the Einstein relation $D_s^L=kT/f$, we find after rearrangement

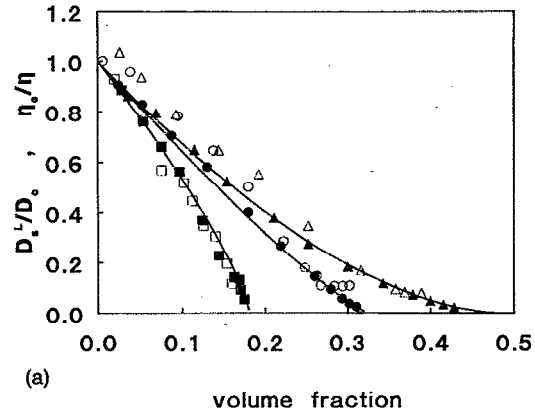

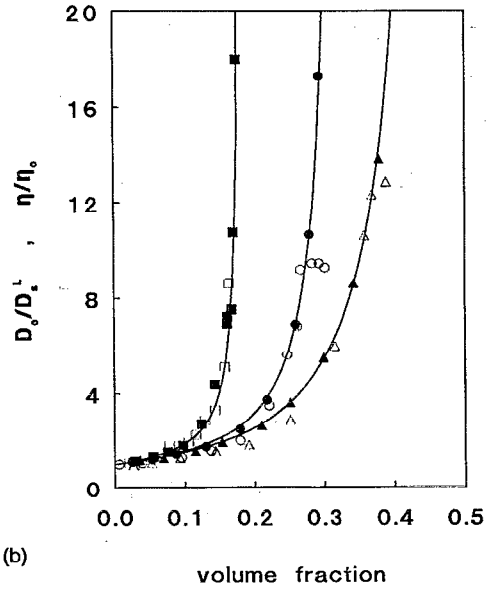

FIG. 7. (a) and (b) The same as Fig. 6, but with volume fractions of D_s^L rescaled with factors 0.826, 0.920, and 0.878 for the 0, 0.001, and 0.1 M systems, respectively.

$$\frac{D_0/D_s^L-1}{\eta/\eta_0-1}=\nu/6. \tag{37}$$

We interpolated the η_0/η curves to evaluate ν at the volume fractions, where D_s^L had been measured and obtained Fig. 8. Of course for low volume fractions, the quotient in Eq. (37) contains a very large error, so we do not display those data. It is seen that ν takes on a value of ~3 for a large range of volume fractions except close to freezing, where ν tends to be somewhat smaller. The values of ν are smaller than 4, a fact that cannot be understood on the basis of the simple intuitive picture described above. However, for the self-diffusion of an atom or a molecule in a pure molecular liquid, the value of ν, defined as $D_s kT/\pi\eta a$, is found experimentally to be ~3 as well.[9] This seems to point to yet another analogy between colloidal and molecular systems.

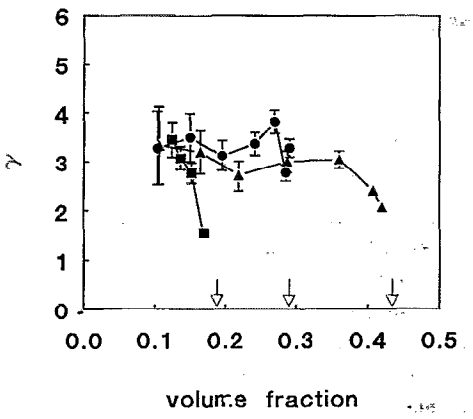

FIG. 8. Factor ν as defined by Eq. (37). (Squares) 0; (circles) 0.001; and (triangles) 0.1 M. Arrows indicate the respective freezing volume fractions.

V. CONCLUDING REMARKS

We measured the long-time self-diffusion coefficient D_s^L and the low-shear limiting viscosity $\eta_{\dot{\gamma}\to 0}$ of charge stabilized colloidal silica spheres dispersed in dimethylformamide with various ionic strengths. Although D_0/D_s^L and η/η_0 show a qualitatively similar dependence on volume fraction, the results do not satisfy a simple Stokes–Einstein-like relation between the two quantities as is often anticipated in the literature. In view of the experimental result obtained earlier that for hard spheres such a relation seems quite accurate, it could be expected that its validity increases as the particles approach hard-sphere-like behavior. However, such a trend could not be demonstrated on decreasing the range of electrostatic repulsion. It would seem therefore that there is no fundamental reason for the existence of a generalized Stokes–Einstein relation such as in molecular systems. However, it was possible to describe the data reasonably well up to volume fractions close to freezing using the modified Eq. (36) with $\nu \approx 3$ for the friction factor.

In addition, we were able to demonstrate convincingly a smooth decrease of D_s^L with volume fraction up to the freezing volume fraction ϕ_f at which point a constant value was reached that persists throughout the coexistence region. This constant value was only about a factor of 10 smaller than the free diffusion coefficient. This relatively high mobility could very well explain the very rapid crystallization (seconds to minutes) that is often observed in these types of dispersions.

ACKNOWLEDGMENTS

This work is part of the research program of the Foundation for Fundamental Research of Matter (FOM) with financial support from the Netherlands Organization for Scientific Research (NWO). The authors wish to thank Dr. B. Tinland for assistance during some of the FRAP measurements.

[1] M. M. Kops-Werkhoven and H. M. Fijnaut, J. Chem. Phys. **77**, 2242 (1982).
[2] W. van Megen and S. M. Underwood, J. Chem. Phys. **91**, 552 (1989).
[3] R. H. Ottewill and N. St. J. Williams, Nature **325**, 232 (1987).
[4] W. Härtl, H. Versmold, and X. Zhang-Heider, Ber. Bunsenges. Phys. Chem. **95**, 1105 (1991).
[5] S. Gorti, L. Plank, and B. R. Ware, J. Chem. Phys. **81**, 909 (1984).
[6] A. van Blaaderen, J. Peetermans, G. Maret, and J. K. G. Dhont, J. Chem. Phys. **96**, 4591 (1992).
[7] A. Einstein, *Investigations on the Theory of the Brownian Motion* (Dover, New York, 1956).
[8] D. Chatenay, W. Urbach, R. Messager, and D. Langevin, J. Chem. Phys. **86**, 2343 (1986).
[9] H. J. V. Tyrrell, *Diffusion and Heat Flow in Liquids* (Butterworth, London, 1961), pp. 159–160.
[10] R. Zwanzig, J. Chem. Phys. **79**, 4507 (1983).
[11] U. Balucani, R. Vallauri, and T. Gaskell, Ber. Bunsenges. Phys. Chem. **94**, 261 (1990).
[12] J. Davoust, P. F. Devaux, and L. Leger, EMBO Journal **1**, 1233 (1982).
[13] G. K. Batchelor, J. Fluid Mech. **131**, 155 (1983).
[14] B. Cichocki and B. U. Felderhof, J. Chem. Phys. **89**, 3705 (1988).
[15] J. A. Leegwater and G. Szamel, Phys. Rev. A **46**, 4999 (1992).
[16] (a) B. Cichocki and K. Hinsen, Physica A **166**, 473 (1990); (b) **187**, 133 (1992).
[17] M. Medina-Noyola, Phys. Rev. Lett. **60**, 2705 (1988).
[18] E. J. W. Verwey and J. Th. G. Overbeek, *Theory of the Stability of Lyophobic Colloids* (Elsevier, Amsterdam, 1948).
[19] D. Axelrod, D. E. Koppel, J. Schlessinger, E. Elson, and W. W. Webb, Biophys. J. **16**, 1055 (1976).
[20] F. Lanni and B. R. Ware, Rev. Sci. Instrum. **53**, 905 (1982).
[21] W. Stöber, A. Fink, and E. Bohn, J. Colloid Interface Sci. **26**, 62 (1968).
[22] A. van Blaaderen and A. Vrij, Langmuir **8**, 2921 (1992).
[23] J. Prue and P. J. Sherrington, Trans. Faraday Soc. **57**, 1795 (1961).
[24] R. J. Hunter, *Zeta Potential in Colloid Science* (Academic, London, 1981).
[25] S. E. Paulin and B. J. Ackerson, Phys. Rev. Lett. **64**, 2663 (1990).
[26] W. G. Hoover and F. H. Ree, J. Chem. Phys. **49**, 3609 (1968).
[27] S. Hachisu, Y. Kobayashi, and A. Kose, J. Colloid Interface Sci. **42**, 342 (1973).
[28] A. Grabbe and R. G. Horn, J. Colloid Interface Sci., **157**, 375 (1993).
[29] R. S. Kittila, *Dimethylformamide: Chemical Uses* (Du Pont de Nemours, Wilmington, Delaware, 1967).
[30] J. C. van der Werff and C. G. de Kruif, J. Rheol. **33**, 421 (1989).